Can we observe near-inertial waves by using lowered Acoustic Doppler Current Profiler?

K. Katsumata*

December 5, 2022

Abstract

Feasibility of observing near-inertial waves with a single cast of a lowered Acoustic Doppler Current Profiler is quantitatively assessed in simulated Garrett-Munk internal waves. Because the inertial period is shorter in higher latitudes and the interval between the up- and downcasts is longer in shallower depths, the performance of the estimator is better in higher latitudes at shallower depths. Even in the best conditions, however, the estimates are contaminated by relative uncertainties greater than 100%. It is not feasible to estimate near-inertial waves accurately using a LADCP cast. Nevertheless, repeated casts at one station are capable of resolving typical near-inertial waves.

1 Introduction

Measurement of horizontal current velocity with Acoustic Doppler Current profilers attached to a Conductivity Temperature Depth (CTD) profiler is routine since the data processing methods have been established (Fischer and Visbeck, 1993; Visbeck, 2002). The sensors on a CTD are designed to be used with a descent or ascent speed of approximately 1 m/s and one cast of CTD often takes hours at deep water. Two profiles of horizontal current velocity measured in up- and downcasts or in two casts at an interval of several hours often show totally different profiles. A typical example is found in Figure 17a of Richardson et al (1979).

*RIGC, JAMSTEC, k.katsumata@jamstec.go.jp

As is often demonstrated in frequency power spectrum of velocity field (e.g. Fu, 1981), the power of horizontal velocity or kinetic energy shows a conspicuous peak at the inertial frequency.

These two facts suggest a possibility that variation of horizontal velocity at or near the inertial frequency can be measured by an LADCP cast in deep waters. Multiple velocity measurements have been used to study internal waves by Sanford (1975) and his collaborators (e.g. Leaman and Sanford, 1975; D'Asaro and Perkins, 1984; Kunze and Sanford, 1984). The question here is if it is possible to reduce the number of samples to as few as two in one inertial period. Multiple inertial periods have been used for coarse ($\sim$ 6 hours) sampling (e.g. Dosser and Rainville, 2016).

The number of measurements of near-inertial gravity waves would dramatically increase if each of these LADCP casts resolves the near-inertial waves. These waves play important roles in energy transfer from wind to interior ocean and in concurrent mixing (Alford et al, 2016). Nevertheless, the near-inertial waves are difficult to observe due mainly to two reasons. One is that these waves occur intermittently in space and time (e.g. Yu et al, 2022). Most of large amplitude near-inertial waves in the upper ocean are observed in response to surface events such as passage of tropical cyclones. The other reason is that these waves propagate almost horizontally, as prescribed by the dispersion relation (see later Equation 2), with water parcel oscillating in the horizontal plane such that they are not visible in temperature and salinity profiles unless the inertial wind has some rotary component and supports Ekman pumping at the inertial period (Gill, 1984).

In this short note, I investigate if it is possible to estimate the amplitude and phase of near-inertial waves from one LADCP cast. At one depth, two components of horizontal velocity are available (usually northward and eastward). There are two measurements at one depth, one at downcast another at upcast. In theory, these four data are just sufficient to determine four unknowns once its frequency is assumed to be inertial (e.g. amplitude and phase of upward propagating and downward propagating waves). The result, however, proves to be negative – it is not possible to observe near-inertial waves in typical oceanic internal wave field. Repeated casts are shown necessary to quantitatively estimate wave properties such as amplitude and phases of the near-inertial waves.

2 Method

2.1 Simulated internal wave field

The Garrett-Munk (GM) model of the oceanic internal waves (Garrett and Munk, 1972, 1975; Munk, 1981) is used to simulate the velocity field, in which a virtual LADCP measures the inertial waves. The GM model prescribes the amplitudes of internal waves at given wavenumbers (two components in the horizontal directions and one in the vertical) and frequencies. The phases are given by a quasi-random number generator. A wave in a box with zonal and meridional horizontal extents of $L_x = L_y$ =200 km and a vertical depth of L_z =4000 m has zonal and meridional wave lengths of L_x/n_x and L_y/n_y, respectively, where n_x and n_y are integers from 1 to 100. The vertical wavenumber m is given by the vertical mode number j under the WKB approximation

$$m = \frac{\pi}{b}\frac{N}{N_0}j, \tag{1}$$

where $b = 1300$m is the vertical length scale and N is the buoyancy frequency scaled by $N_0 = 5.2 \times 10^{-3}$ s^{-1}. Vertical modes from 1 to 100 are used. These wavenumbers fix a frequency ω by the dispersion relation

$$\omega = \pm\sqrt{\frac{k^2+l^2}{k^2+l^2+m^2}N^2 + \frac{m^2}{k^2+l^2+m^2}f^2}. \tag{2}$$

Half of the modes are randomly chosen to have positive frequencies and the other half negative frequencies. Finally, the velocity power $\langle u^2+v^2\rangle$ at this frequency and vertical mode j is given by

$$\langle u^2+v^2\rangle = \int_f^N \sum_j b^2 N_0 N \frac{\omega^2+f^2}{\omega^2} B(\omega)H(j)E_0 \mathrm{d}\omega \tag{3}$$

which is the 1981 version (Munk, 1981) of the GM spectrum. Here, $B(\omega) = 2\pi^{-1}f\omega^{-1}(\omega^2-f^2)^{-1/2}$, $H(j) = (j^2+j_*^2)^{-1}/\Sigma_1^{100}(j^2+j_*^2)^{-1}$, $E_0 = 6.3\times10^{-5}$, and $j^* = 3$. We truncate the vertical summation at $j = 100$. We did not include the horizontal mode zero (i.e. uniformly moving field, representing waves with scales larger than the box size).

We expect wind events add near-inertial waves on top of the background GM spectrum. For quantitative analysis, it is necessary to be able to estimate the amplitude of the near-inertial waves such that these enhanced waves can be distinguished from the background. To

test this ability, we performed experiments with enhanced near-inertial wave. Here, near-inertial waves are defined as waves with frequency $\omega < 1.05f$. From these near-inertial modes within the GM spectrum, half modes are randomly chosen and their amplitudes are increased by a factor $F > 1$. The phases of these enhanced waves are assigned randomly within a range of $\Phi \pm \Delta\Phi$, where Φ is a randomly chosen central phase and $\Delta\Phi = \pi/10$ is the bandwidth. By restricting the phase within a $2\Delta\Phi$ bandwidth, the enhanced near-inertial waves appear as a wave packet, mimicking the responses from wind events (Figure 1). Three cases of amplification F are used; $a = 5$, 10, and 15 dB where $a(\mathrm{dB}) = 10 \times \log_{10} F$. This decibel (dB) notation was used to facilitate comparison with observation by Fu (1981).

2.2 Virtual measurements

A virtual LADCP measures the simulated velocity fields. We do not consider measurement errors here. For downcast at time $t = t_d$, if the horizontal velocity is totally inertial with an eastward amplitude $\sqrt{u_s^2 + u_c^2}$ and a northward amplitude $\sqrt{v_s^2 + v_c^2}$,

$$\begin{aligned} u_d &= u_s \sin f t_d + u_c \cos f t_d \\ v_d &= v_s \sin f t_d + v_c \cos f t_d \end{aligned} \tag{4}$$

and for upcast at $t = t_u$

$$\begin{aligned} u_u &= u_s \sin f t_u + u_c \cos f t_u \\ v_u &= v_s \sin f t_u + v_c \cos f t_u \end{aligned} \tag{5}$$

Note that as the expansion $\sin(f + \delta f)t = \cos(\delta f \cdot t) \sin ft + \sin(\delta f \cdot t) \cos ft$ shows, the fit does not distinguish a small deviation of frequency from inertial ($\delta f \ll f$) from a small change in amplitude. The unknown zonal velocity amplitudes oscillating at the inertial frequency are determined as

$$\begin{pmatrix} u_s \\ u_c \end{pmatrix} = \frac{1}{D} \begin{pmatrix} \cos f t_u & -\cos f t_d \\ -\sin f t_u & \sin f t_d \end{pmatrix} \begin{pmatrix} u_d \\ u_u \end{pmatrix}, \tag{6}$$

where

$$D = \sin f(t_u - t_d). \tag{7}$$

The meridional velocity amplitudes v_s, v_c are determined similarly. It is noted that the estimation performs best when the upcast and

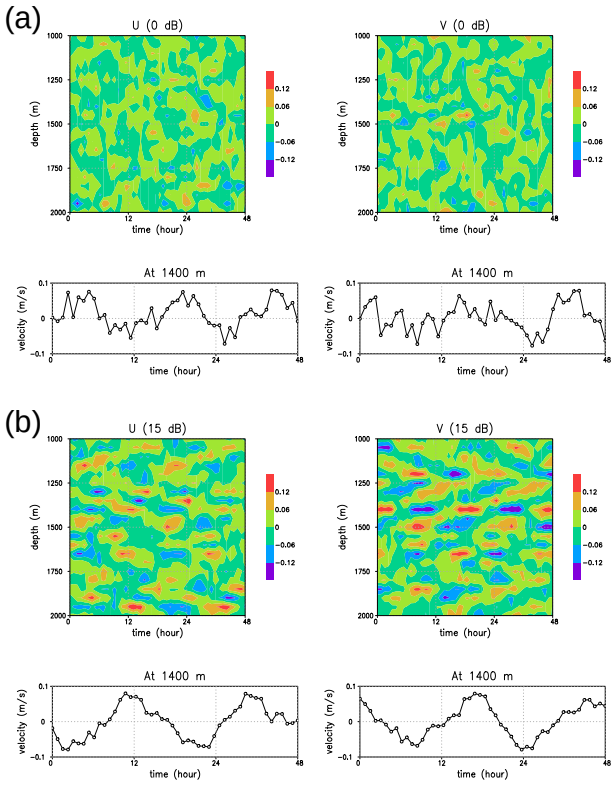

Figure 1: (a) Simulated internal wave field at 30°N latitude. The top 2 panels show the zonal and meridional component, respectively, in 48 hours (horizontal axis) at depths (vertical axis) between 1000 and 2000 m. The bottom 2 panels are a time series at a fixed depth of 1400 m. (b) Simulated internal waves with near-inertial waves enhanced by a multiplicative factor of 15 dB (= 31.6). Both upward and downward propagating near-inertial wave packets are visible between 1000 and 1500 m depth.

downcast is separated by an interval of a quarter of the inertial period $t_u - t_d = \pi/(2f)$, instead of apparently optimal half the period $t_u - t_d = \pi/f$. The following example shows that the half inertial period is not actually the optimal. At a latitude of 30° N, the inertial period is 24 hours. If an zonal speed of 1 m/s is observed at T =0 hours and −1 m/s at T =12 hours. If the phase ψ of an inertial wave $u = A\sin((2\pi/f)t + \psi)$ is $\psi = \pi/2$, $A = 1$ m/s, but for $\psi = \pi/4$, $A = \sqrt{2}$ m/s. We thus need the linear independence of the upcast and downcast, $D \neq 0$, to estimate both phase and amplitude.

From (7), it is seen that the solution becomes unstable as the interval between upcast and downcast, $t_u - t_d$, at a particular depth (henceforth called measurement interval T_I) becomes short compared to the inertial period $2\pi/f$. In order to examine this relationship, we vary the Coriolis frequency f and the measurement interval T_I. The Coriolis frequency is varied by setting the latitude at 10, 20, 30, 40, and 50 degrees north. In CTD casts, the ascend and descent speed of the sensor is generally set at approximately 1 m/s. In a typical cast at a 4000 m depth, the measurement interval T_I at 1000m depth is $(4000 - 1000) \times 2 = 6000$ seconds = 100 minutes. The measurement interval T_I is varied at 10, 20, ..., 100 minutes. We assume effects of the background stratification is accounted for by the WKB approximation, i.e., the horizontal velocity scaled by $\sqrt{N}$ and the vertical wavenumber by (1).

A time series of horizontal velocity is extracted from the simulation described in the previous Section 2.1 at a depth of 2000 m with a duration of 48 hours and a resolution of 1 minute. Although we add the near-inertial waves, the waves do not necessarily increase the amplitude at the observation depth as the near-inertial waves form a packet which does not necessarily go through the 2000 m depth (Figure 1). We therefore define the true near-inertial wave amplitude A by fitting a sinusoidal curve to the 48 hour timeseries using the least squares method, instead of using the spectral power. From the timeseries, a virtual measurement is made by choosing a velocity couple at $t = T_0$ minute and at $t = T_0 + T_I$ minute. An ensemble of 24 such "measurements" are thus made from a single timeseries with T_I =10, 20, ... 100 minutes. We simulate 10 timeseries and repeated the process for each simulated time series.

3 Results

Twenty-four virtual measurements are made from each of 10 simulated timeseries with different measurement intervals T_I and inertial wave amplitudes A. The experiment is repeated at five different latitudes of 10, 20, ..., 50 degrees. From each virtual measurements, amplitudes of each sinusoidal functions u_s, u_c, v_s, v_c are calculated using (6). By denoting the "true" (i.e. estimated by the least squares fit to the simulated timeseries) amplitudes by the superscript $*$, we calculate root-mean-square error σ for 24 virtual measurements of, say u_s, as

$$\sigma(u_s) = \left(\frac{1}{24} \sum_{i=1}^{24} (u_s^{(i)} - u_s^*)^2 \right)^{1/2} . \tag{8}$$

The behaviour of $\sigma(u_s), \sigma(u_c), \sigma(v_s)$, and $\sigma(v_c)$ are shown in Figure 2. As expected from (7), the error decreases with the measurement interval T_I, but only slowly. For example, at 40° latitude, doubling T_I from 40 to 80 minutes leads to only $\sim 30\%$ decrease in σ (average RMS = 0.10 m/s for $T_I = 40$ minute, 0.07 m/s for $T_I = 80$ minute). The distribution of different markers indicate that the error is not sensitive to the true amplitude. The smallest error is found for the longest measurement interval $T_I = 100$ minutes as expected from the largest D in (6). Even at these conditions, however, it is seen that the error is of the same order as the true amplitude. This is a hopeless performance of the present method, suggesting that the present method cannot be used for qualitative analysis. Despite the large error, the estimates are not biased (figure not shown).

The Doppler sensors of LADCP output vertical shear of the horizontal current, which is processed with ship position and pressure timeseries to estimate the horizontal currents. Some instruments (e.g. expendable current profiler) can only measure vertical shear of horizontal currents. It is a simple modification to obtain the simulated field of vertical shear of horizontal velocity associated with the GM internal wave – multiplication of horizontal velocity by the vertical wave number. Virtual observation was made to the vertical shear field and the result (Figure 3) shows that extraction of near-inertial waves are even more difficult with vertical shear than with horizontal velocity.

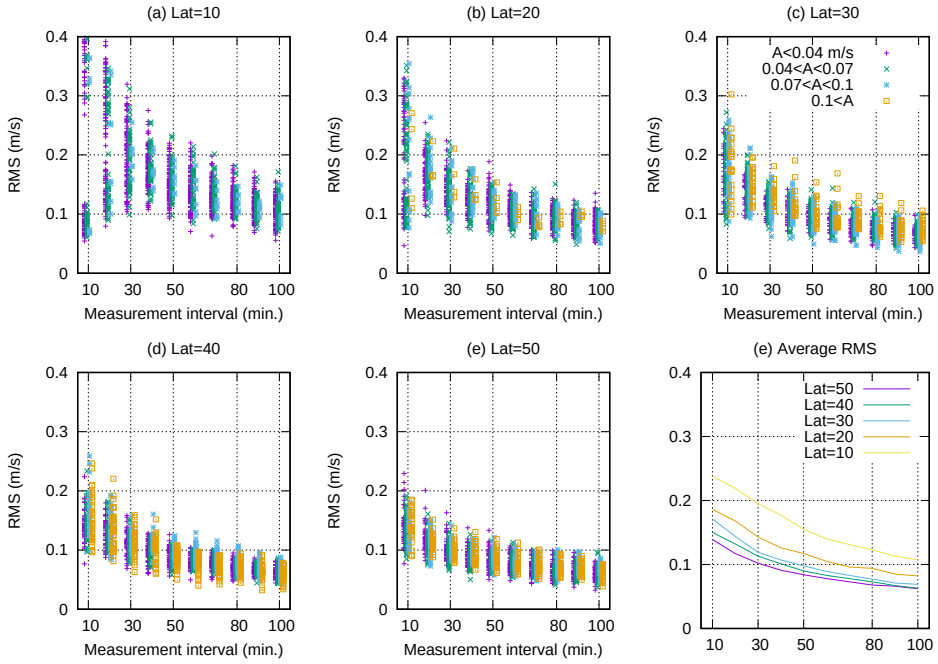

Figure 2: Distribution of root-mean-square error in estimated amplitudes (u_s, u_c, v_s, and v_c) for 10 simulated wavefield at latitude of (a) 10°N, (b) 20°N, (c) 30°N, (d) 40°N, and (e) 50°N, and (f) shows the average of the markers at each latitude and measurement interval. The abscissa shows the measurement interval T_I with leftmost $T_I = 10$ minutes, the ordinate the root-mean-square error. The color and shape of the markers indicate the amplitude of the true component ($A = \sqrt{u_s^{*2} + u_c^{*2} + v_s^{*2} + v_c^{*2}}$). All components, both zonal (u) and meridional (v), and both cosine (u_c, v_c) and sine (u_s, v_s), are plotted without distinction.

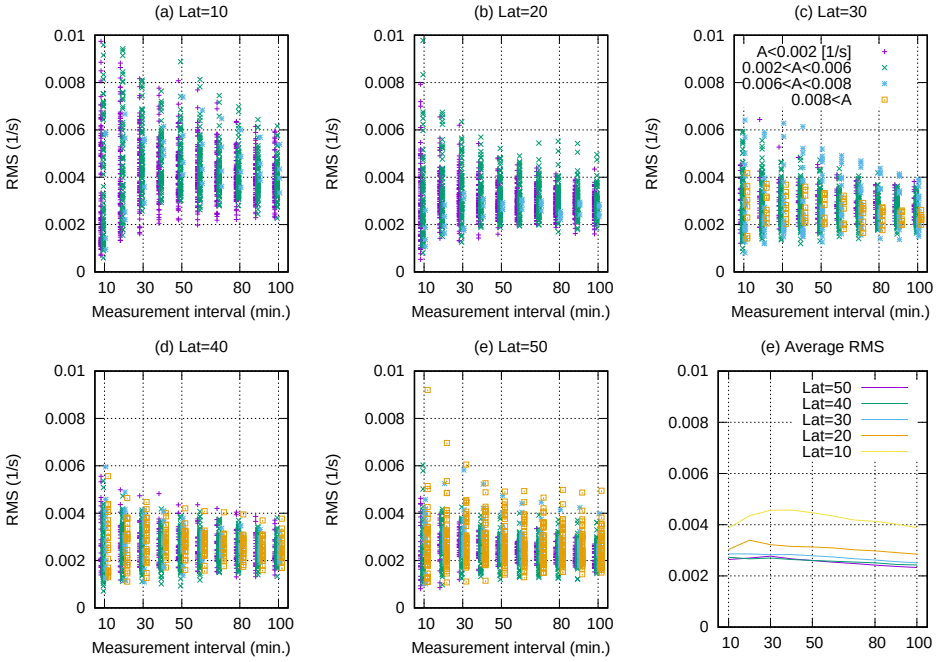

Figure 3: Distribution of root-mean-square error in estimated shear amplitudes ($\partial u_s/\partial z, \partial u_c/\partial z, \partial v_s/\partial z$, and $\partial v_c/\partial z$) for 10 simulated wavefield at latitude of (a) 10°N, (b) 20°N, (c) 30°N, (d) 40°N, and (e) 50°N, and (f) shows the average of the markers at each latitude and measurement interval. The abscissa shows the measurement interval t_I with leftmost $t_I = 10$ minutes, the ordinate the root-mean-square error. The color and shape of the markers indicate the amplitude of the true component ($A = \sqrt{(\partial u_s^*/\partial z)^2 + (\partial u_c^*/\partial z)^2 + (\partial v_s^*/\partial z)^2 + (\partial v_c^*/\partial z)^2}$). All components, both zonal (u) and meridional (v), and both cosine (u_c, v_c) and sine (u_s, v_s), are plotted without distinction.

4 Discussion and Conclusions

Although the estimation of horizontal velocity oscillation at the inertial frequency is possible in theory, the simulated virtual observation shows that the estimated coefficients of the sinusoidal functions are contaminated by errors with the magnitude comparable to the signal. From the coefficients of sine and cosine, say b and c, the amplitude Φ and phase θ are given as $\Phi^2 = b^2 + c^2$ and $\tan\theta = b/c$, respectively. The magnitude of the error for each quantity is given as

$$\begin{aligned} \frac{(\delta\Phi)^2}{\Phi^2} &= \frac{b^2(\delta b)^2 + c^2(\delta c)^2}{\Phi^4} \\ &\sim \frac{b^2 b^2 + b^2 b^2}{(b^2+b^2)^2} \\ &\sim \frac{1}{2} \end{aligned} \tag{9}$$

and

$$\begin{aligned} (\delta\theta)^2 &= \frac{c^2(\delta b)^2 + b^2(\delta c)^2}{\Phi^4} \\ &\sim \frac{b^2 b^2 + b^2 b^2}{(b^2+b^2)^2} \\ &\sim \frac{1}{2} \sim \frac{\pi}{6} \end{aligned} \tag{10}$$

where δ signifies the uncertainty and we assumed the uncertainty is of a similar magnitude as the signal, i.e., $b \sim \delta b \sim c \sim \delta c$. In other words, the relative error of amplitude is as bad as $1/\sqrt{2} \approx 0.7$ and the absolute error of phase is $\pi/6$.

One way to reduce the error is to combine multiple observations that are statistically independent. Spatially, two observations can be regarded independent if the two are separated by a distance greater than the coherence length scale. As shown in Garrett and Munk (1975), the vertical coherence for a separation Y for fixed measurements (referred to as "moored vertical coherence" or MVC) is given by

$$\mathrm{MVC} = \int_0^\infty H(j)\cos(j\pi\lambda Y)\frac{\mathrm{d}j}{j^*}, \tag{11}$$

where $H(j)$ is defined in Equation (3). Similarly, the horizontal coherence ("moored horizontal coherence" or MHC) for a separation X

by

$$\mathrm{MHC} = \int_0^\infty H(\lambda) J_0(j\pi\sqrt{\omega^2 - f^2} X \frac{\mathrm{d}j}{j^*}, \tag{12}$$

where J_0 is the Bessel function. Numerical evaluation for modes j =1 to 100 gives the vertical and horizontal scale lengths of 300 m and 220 km, respectively, as the first zero crossing of the coherence curves. We set $\omega = 1.04f$ for (12). From a year-long mooring observation, Yu et al (2022) obtained a mean vertical and horizontal wavelengths of near-inertial waves with mean frequency $(1.039 \pm 0.018)f$ are 652 ± 185 m and 79 ± 28 km, respectively. These wavelengths suggest that it is not possible to obtain more than several independent observations in one wavelength by the present method. We conclude that LADCP cannot be used to observe near-inertial waves with the present method.

Another approach to investigate the horizontal velocity measured by LADCP is through the use of the vertical wavenumber spectra. This is equivalent to assuming a range of vertical wavelengths for near-inertial waves. Waterhouse et al (2022) employed this method, using a vertical wavelength band of between 100 m and 320 m for LADCP, and showed that globally downward going energy is greater than upward going in the upper 600 m and that no obvious asymmetry found below that depth.

Given the large errors in one cast of LADCP measurement, repeated LADCP casts (often called yo-yo casts) should be employed if one attempts to retain the frequency information rather than assuming the vertical scale of the horizontal velocity measurements. Expendable current profilers (XCP), which measure vertical shear of horizontal velocity can be an efficient alternative to LADCP for repeat measurements, but we note that the vertical shear cannot substitute the horizontal velocity measurement in typical internal wave fields (Figure 3). We also note that the measurement depth of XCP is limited (< 1000 m depth). If horizontal velocity in an internal wave field is measured N times, the error can be reduced by a factor of $\sqrt{N}$. At 30° latitude, where the inertial period is 24 hours, Figure 2 shows that at this latitude, an measurement interval T_I longer than 50 minutes has an error of 0.1 ms^{-1}. At 4000 m depth, a CTD cast without water sampling would take 8000 seconds or approximately 2.5 hours. Four casts within 24 hours are sufficient to resolve the amplitude by 0.05 ms^{-1} and the phase by $\pi/12 = 1$ hour. As demonstrated by mooring observation (Yu et al, 2022), the internal waves below mixed layers are observed in response to wind events. The wave propagates at a

speed of 50 to 80 m/day (Yu et al, 2022). It is quite plausible to observe by ship these near-inertial waves at around 500 m depth after 6 to 10 days after a storm. This sort of event dependent observation is difficult to plan ahead but can serve as one possible option when a cruise fortuitously end up with some extra time offshore.

Acknowledgments

This work was supported by JSPS KAKENHI Grant-in-Aid for Scientific Research (C) 20K04076. The manuscript was submitted to *J.Oceanogr* and was not accepted for publication. Comments from two reviewers were, however, much appreciated and the current version reflects revisions in response to the comments.

Declarations

The author declares no competing interests.

References

Alford MH, MacKinnon JA, Simmons HL, et al (2016) Near-inertial internal gravity waves in the ocean. Annual review of marine science 8:95–123

D'Asaro EA, Perkins H (1984) A Near-Inertial Internal Wave Spectrum for the Sargasso Sea in Late Summer. Journal of Physical Oceanography, 14(3): 489–505

Dosser, HV, Rainville L (2016) Dynamics of the Changing Near-Inertial Internal Wave Field in the Arctic Ocean. Journal of Physical Oceanography 46(2):395–415

Fischer J, Visbeck M (1993) Deep velocity profiling with self-contained adcps. Journal of atmospheric and oceanic technology 10(5):764–773

Fu LL (1981) Observations and models of inertial waves in the deep ocean. Reviews of Geophysics 19(1):141–170

Garrett C, Munk W (1972) Space-time scales of internal waves. Geophysical Fluid Dynamics 3(3):225–264

Garrett C, Munk W (1975) Space-time scales of internal waves: A progress report. Journal of Geophysical Research 80(3):291–297

Gill AE (184) On the behavior of internal waves in the wakes of storms. Journal of Physical Oceanography, 14(7): 1129–1151

Kunze E, Sanford TB (1984) Observations of near-inertial waves in a front. Journal of Physical Oceanography 14(3):566–581

Leaman, KD, Sanford TB (1975) Vertical energy propagation of inertial waves: A vector spectral analysis of velocity profiles. Journal of Geophysical Research 80(15):1975–1978

Munk WH (1981) Internal waves and small-scale processes. Evolution of physical oceanography pp 264–291

Richardson PL, Maillard C, Stanford TB (1979) The physical structure and life history of cyclonic gulf stream ring allen. Journal of Geophysical Research: Oceans 84(C12):7727–7741

Sanford, TB (1975) Observations of the vertical structure of internal waves. Journal of Geophysical Research 80(27):3861 – 3871

Visbeck M (2002) Deep velocity profiling using lowered acoustic doppler current profilers: Bottom track and inverse solutions. Journal of Atmospheric and Oceanic Technology 19(5):794 – 807

Waterhouse AF, Hennon T, Kunze E, et al (2022) Global observations of rotary-with-depth shear spectra. Journal of Physical Oceanography 52(12):3241–3258

Yu X, Naveira Garabato AC, Vic C, et al (2022) Observed equatorward propagation and chimney effect of near-inertial waves in the midlatitude ocean. Geophysical Research Letters 49(13):e2022GL098,522